Applied Catalysis B: Environmental 309 (2022) 121257

Contents lists available at ScienceDirect

Applied Catalysis B: Environmental

journal homepage: www.elsevier.com/locate/apcatb

Organic dyes with multi-branched structures for highly efficient photocatalytic hydrogen evolution under visible-light irradiation

Siwei Liu [a], Peixuan Lin [a], Meng Wu [b], Zhi-An Lan [b,d], Hangyu Zhuzhang [b], Mengmeng Han [a], Yunhao Fan [a], Xiong Chen [b,*], Xinchen Wang [b,*], Qianqian Li [a,*], Zhen Li [a,c,**]

[a] Hubei Key Lab on Organic and Polymeric Opto-Electronic Materials, Sauvage Center for Molecular Sciences, Department of Chemistry, Wuhan University, Wuhan 430072, China
[b] State Key Laboratory of Photocatalysis on Energy and Environment, College of Chemistry, Fuzhou University, Fuzhou 350116, China
[c] Institute of Molecular Aggregation Science, Tianjin University, Tianjin 300072, China
[d] College of Chemical Engineering, Fuzhou University, Fuzhou 350116, China

ARTICLE INFO

Keywords:
Multi-branched structure
Heterojunction system
Organic dye
Hydrogen evolution
Polymeric carbon nitride (PCN)

ABSTRACT

Direct photocatalytic water splitting is an attractive strategy for clean energy, in which, organic photocatalytic systems with broad light-harvesting region and efficient charge separation are highly desired and still challenging. In this paper, three multi-branched organic dyes were designed and synthesized with dipolar, V-shaped, and octupolar geometries, respectively. The multiple intramolecular charge transfer processes by electronic pull-push effect along the branches can provide more channels for light-harvesting and carrier transporting. Also, the interactions with polymeric carbon nitride (PCN) can be optimized by multiple anchoring units and defect filling effect, resulting in the gradually enhanced photocatalytic hydrogen evolution performance with the increased number of branches. Accordingly, the highest one of 996.9 μmol h^{-1} was achieved, which is over 40-folders that of PCN/Pt (24.8 μmol h^{-1}) under the same conditions. It provides an efficient strategy for molecular design of organic dyes as photocatalyst, promoting development of PHE system from the molecular level.

1. Introduction

Photocatalytic hydrogen evolution (PHE) has become one of the most popular research topics for the increasingly serious energy and environmental crisis [1–8]. Among various photocatalytic systems, polymeric carbon nitride (PCN) as an emerging and promising organic semiconductor, has been widely applied for its low cost, simple preparation method and high chemical stability [9–12]. However, the short absorption wavelength (<460 nm) limits the light-harvesting ability, and the charge recombination is usually generated for the high exciton binding energy and low dissociation probability, resulting in the decreased solar-to-hydrogen conversion [13–17]. Thus, researches for organic photocatalytic systems with broad light-harvesting region and efficient separation of photogenerated charge carriers are highly desired and still challenging [18–25]. Recently, modification of PCN with organic dyes is proved as an efficient strategy to improve PHE performance by the extended absorption spectra and enlarged interfacial junction [26–28]. For instance, Tian and co-worker reported a series of *N*-annulated perylene derivatives with the extended absorption to 700 nm, which exhibited PHE rate of 11.8 mmol h^{-1} g^{-1} with the combination of PCN [29]. Also, organic dye bearing triphenylamine (TPA) and diazosulfide units with strong intramolecular charge transfer (ICT) effect demonstrated improved PHE performance of 20.1 mmol h^{-1} g^{-1} [30]. Considering the key role of organic dyes, it is essential to optimize their molecular structures to enhance PHE activity by the well-organized light-harvesting, charge separation and transfer processes [31–34].

Generally, organic dyes consisted of an electron donor (D), a π-conjugated bridge and an electron acceptor (A), and the resultant D-π-A structure with electronic pull-push effect is beneficial to ICT process, resulting in the strong light-harvesting ability [35–39]. Compared to linear molecules, branched ones with V-shaped designs (A-π-D-π-A or D-π-A-π-D), or octupolar designs ((D-π-A)$_3$), may exhibit a strong cooperative effect among multi-branches by their interactions and extended electronic coupling, as proved by the significant improvement of their

* Corresponding authors.
** Corresponding author at: Hubei Key Lab on Organic and Polymeric Opto-Electronic Materials, Sauvage Center for Molecular Sciences, Department of Chemistry, Wuhan University, Wuhan 430072, China.
E-mail addresses: chenxiong987@fzu.edu.cn (X. Chen), xcwang@fzu.edu.cn (X. Wang), liqianqian@whu.edu.cn (Q. Li), lizhen@whu.edu.cn (Z. Li).

https://doi.org/10.1016/j.apcatb.2022.121257
Received 13 December 2021; Received in revised form 30 January 2022; Accepted 23 February 2022
Available online 4 March 2022

optical properties [40–45]. However, until now, the multi-branched structures of organic molecules are seldom reported in PHE systems, regardless of the unique properties upon the excitation by visible-light irradiation [46–49].

Considering with the above points, organic dyes bearing different branched structures have been synthesized and investigated. The number of branches increased from one to two, then to three by the introduction of linear chromophore pieces along different axes to TPA core, yielding the dipolar (**LI-151**), V-shaped (**LI-152**), and octupolar (**LI-153**) geometries, respectively. Moreover, carboxylic acid as the ending unit in each axe can act as the active moiety to promote the anchored and dispersed process to PCN system. Accordingly, the PCN/organic dyes exhibited the extended light harvesting region from ultraviolet to visible light. Among them, PCN modified with three-branched dye **LI-153** shows the highest PHE with efficiency of 996.9 μmol h^{-1}, 40 times that of the bare PCN (24.8 μmol h^{-1}) under the same conditions. Herein, we would like to present their synthesis, structural characterization, photophyical property, theoretical calculation and PHE performance in detail.

2. Experimental section

2.1. Materials and measurements

Catechol, tributyl(4-hexylthiophen-2-yl)stannane, *N*-bromosuccinimide (NBS), and methyl 4-boronobenzoate were purchased commercially and used directly as received. Compounds **9a**, **9b** and **9c** were synthesized according to literature [50].

^{1}H and ^{13}C NMR spectra were recorded on a Bruker Avance III HD 400 MHz using tetramethylsilane (TMS; $\delta = 0$ ppm) as internal standard. Elemental analyses were performed by an Elementar RARIO EL III elemental analyzer. MALDI-TOF spectra were measured on an AB SCIEX MALDI-TOF/TOF 5800 and tributylammonium salt was used as matrix.

2.2. Photophysical measurements

UV–vis spectra were conducted on a Shimadzu UV-2550 spectrometer. Photoluminescence spectra in solution were performed on a Hitachi F-4600 fluorescence spectrophotometer. Photoluminescence spectra at solid state and photoluminescence quantum yields were measured with a FLS980 spectrometer. The Fourier transform infrared (FTIR) spectra were obtained on a Nicolet IS 10 FT-IR spectrometer with KBr as the diluents in the frequency range of 4000–400 cm^{-1}. UPS spectra were obtained by ThermoFisher ESCALAB XI+ .

2.3. Synthesis of polymeric carbon nitride (PCN) and preparation of PCN/Pt, dye/PCN and dye/PCN/Pt

As a typical synthesis, 10 g of urea was calcined at 550 °C in air for 2 h at a heating rate of 10 °C min^{-1}. The obtained solid was grounded into powder with an agate mortar [51]. PCN powder (500 mg) and $H_2PtCl_6.6H_2O$ was added into a mixture solvent of methanol and water (V/V = 5:1120 mL) in a beaker, and the solution was irradiated under a Xe lamp (300 W) for 3 h, then 3.0 wt% PCN/Pt was obtained by filtration and washed three times by water. PCN (100 mg) and dyes (2 mg) were immersed in a mixture solvent of $CHCl_3$ and MeOH (V/V = 4:1, 10 mL), and stirred at room-temperature in dark for 3 h, then the solution was removed by rotary evaporation to give dye/PCN. Dye/PCN/Pt was obtained by the similar method with PCN/Pt as the source.

2.4. Characterization of PCN, PCN/Pt, dye/PCN and dye/PCN/Pt

The powder X-ray diffraction patterns were recorded by D8 Advanced (Bruker) using Cu-Kα radiation from 10° to 50°. X-ray photoelectron spectroscopy (XPS) data were obtained on ThermoFisher Nexsa instrument with a monochromatized Al Kα line source. Scanning electron microscope (SEM) were obtained in Hitachi S-4800 scanning electron microscope Transmission electron microscopy (TEM) were obtained in JEM-F200 transmission electron microscope and JEM-2010 FEF transmission electron microscope. UV–Vis diffuse reflectance spectra (UV–Vis DRS) were performed on UV-3600 Ultraviolet-Visible-Near Infrared Spectrophotometer MPC-3100. Photoluminescence spectra and lifetimes at solid state were determined by FLS980 spectrometer. Nitrogen adsorption−desorption isotherms were performed at 77 K using Micromeritics ASAP 2460 equipment. Water contact angle were performed at POWERREACH JC2000D contact angle measuring instrument.

2.5. Photoelectrochemical measurements

Photocurrent density curves and EIS were obtained in a conventional three electrode cell by ModuLab XM ECS, using a Pt plate as the counter electrode and an Ag/AgCl (3 M KCl) electrode as the reference electrode. The working electrode was prepared on indium-tin oxide (ITO) glass that was cleaned by sonication in ethanol and acetone for 30 min and dried at 353 K. The boundary of ITO glass was protected using Scotch tape. The sample (5 mg, PCN, PCN/Pt, LI-151/PCN/Pt, LI-152/PCN/Pt or LI-153/PCN/Pt) was dispersed in a mixed solution (0.5 mL, 480 μL of absolute ethanol and 20 μL of Nafion solution) by sonication to get a slurry. The slurry was spread onto pretreated ITO glass. After air-drying, the Scotch tape was unstuck, and the uncoated part of the electrode was isolated with epoxy resin to get a 1 cm × 1 cm film electrode. A Na_2SO_4 solution (0.5 M) was used as the electrolyte. Before testing, the electrolyte was purged with N_2 to remove dissolved oxygen. EIS was determined over the frequency range of 10^{-2}-10^{6} Hz with an ac amplitude of 10 mV at the open circuit voltage.

2.6. Photocatalytic test

Photocatalytic hydrogen evolution arrays were performed in a Pyrex top-irradiation reaction vessel, which was linked to a glass closed gas system. H_2 production was carried out by dispersing 50 mg of photocatalyst powder in an aqueous solution (100 mL) containing triethanolamine (10 vol%) as sacrificial agent. The mixture was evacuated for several times to remove air completely before irradiation under a 300 W Xe-lamp and a water-cooling filter. The wavelength of the incident light was controlled by using a long pass cut-off filter > 420 nm (or other appropriate long pass cut-off filters) for testing wavelength-dependence hydrogen evolution rate of sample. The temperature of the reaction solution was kept at room temperature by a flow of cooling water. The generated gases were analyzed by gas chromatography equipped with a thermal conductive detector (TCD) with argon as the carrier gas.

The apparent quantum yield (AQY) for H_2 evolution was acquired with monochromatic LED lamps with a band-pass filter of 380, 420, 450, 490, and 520 nm. The intensities were 11.3, 17.1, 13.2, 13.0 and 8.5 mW cm^{-2}, respectively (Newport 2936-R optical power meter). The irradiation area was 9 cm^2 for the monochromatic light. Depending on the amount of hydrogen produced by the photocatalytic reaction in 1 h, the AQY value was calculated by the following Equation (1):

$$\mathrm{AQY}\% = \frac{2 \times Number\ \ of\ \ H_2}{Number\ \ of\ \ incident\ \ photons} \times 100\% = \frac{2 \times R_{H_2} \times N_A}{S \times P \times t \times \frac{\lambda}{hc}} \times 100\%$$

Where R_{H_2} denotes the evolved hydrogen amount (μmol), N_A is the Avogadro constant, S is the illumination area, P and λ are the intensity (W cm^{-2}) and wavelength (nm) of the monochromatic light, respectively. t is the irradiation time, h is the Plank constant, and c is the speed of light.

2.7. DFT calculations

DFT calculations were performed on Gaussian 09 program (Revision D09) [52]. The ground state (S0) geometries were optimized with the Becke's three-parameter exchange functional along with the Lee Yang Parr's correlation functional (B3LYP) using 6–31 G(d) basis sets.

2.8. Photoluminescence property of heterojunction and mixing systems

The heterojunction system was fabricated by dispersing 5 mg dye/PCN/Pt into a 5 mL organic solvent ($CHCl_3/CH_3OH$ = 4:1)/aqueous (H_2O/TEOA = 10:1) mixtures with different aqueous fractions. The dye+PCN/Pt system was fabricated by dispersing 4.9 mg PCN/Pt and 0.1 mg dye into a 5 mL organic solvent ($CHCl_3/CH_3OH$ = 4:1)/aqueous (H_2O/TEOA = 10:1) mixtures with different aqueous fractions. The dye system as control group was fabricated by dispersing 0.1 mg dye into a 5 mL organic solvent ($CHCl_3/CH_3OH$ = 4:1)/aqueous (H_2O/TEOA = 10:1) mixtures with different aqueous fractions.

3. Results and discussion

3.1. Molecular design and synthesis

Dye **LI-151**, **LI-152** and **LI-153** (Scheme 1) with different branched structures are constructed by the Suzuki-Miyaura reactions between TPA with different number of borate substituents and the thiophene-benzothiazole-thiophene-phenyl skeletons with bromine atom as the active site. Molecular structures of these compounds are fully confirmed by ^{1}H NMR, ^{13}C NMR, MALDI-TOF(MS), and FTIR spectra, and EA (Fig. S1-S11). As shown in Fig. 1a, the three organic dyes in dilute solution ($CHCl_3/CH_3OH$ (4:1), 1×10^{-5} mol L^{-1}) exhibit the similar absorption peaks at about 380 nm and 480 nm, respectively. The selection of mixture solvent is mainly based on the following two points: (1) good solubility towards organic dyes; (2) suppression of self-association of carboxyl acid moieties as the ending group in organic dyes. Taking dye **LI-153** as the example, it can only be dissolved in THF and $CHCl_3$ solution (Fig. S12). However, the possible association of carboxyl acid moieties can occur in these non-protonic solvents. Thus, methanol as a protic solvent was added into $CHCl_3$ with the optimized ratio of $CHCl_3/CH_3OH$ (4/1) to ensure both the good solubility and suppression of self-association. The peak in the UV region (380 nm) is from π-π transitions, and the latter one (480 nm) in the visible region is due to the ICT effect from TPA (D) to benzothiazole (A) through thiophene as π-conjugated bridge. The molar absorption coefficients of dye **LI-152** and **LI-153** in the visible region exhibit about two-fold and three-fold increase (Table 1, Fig. S13), compared to that of **LI-151**, benefiting to the highly efficient sunlight harvesting. It is mainly due to the multiple ICT processes in V-shaped (**LI-152**) and octupolar (**LI-153**) geometry, as well as the increased number of D-π-A chromophores as the light-harvesting moieties. With the excitation by visible light at wavelength of 515 nm, the three dyes in dilute solution exhibit bright red luminescence with the same emission peak at 658 nm (Fig. 1b). The enhanced

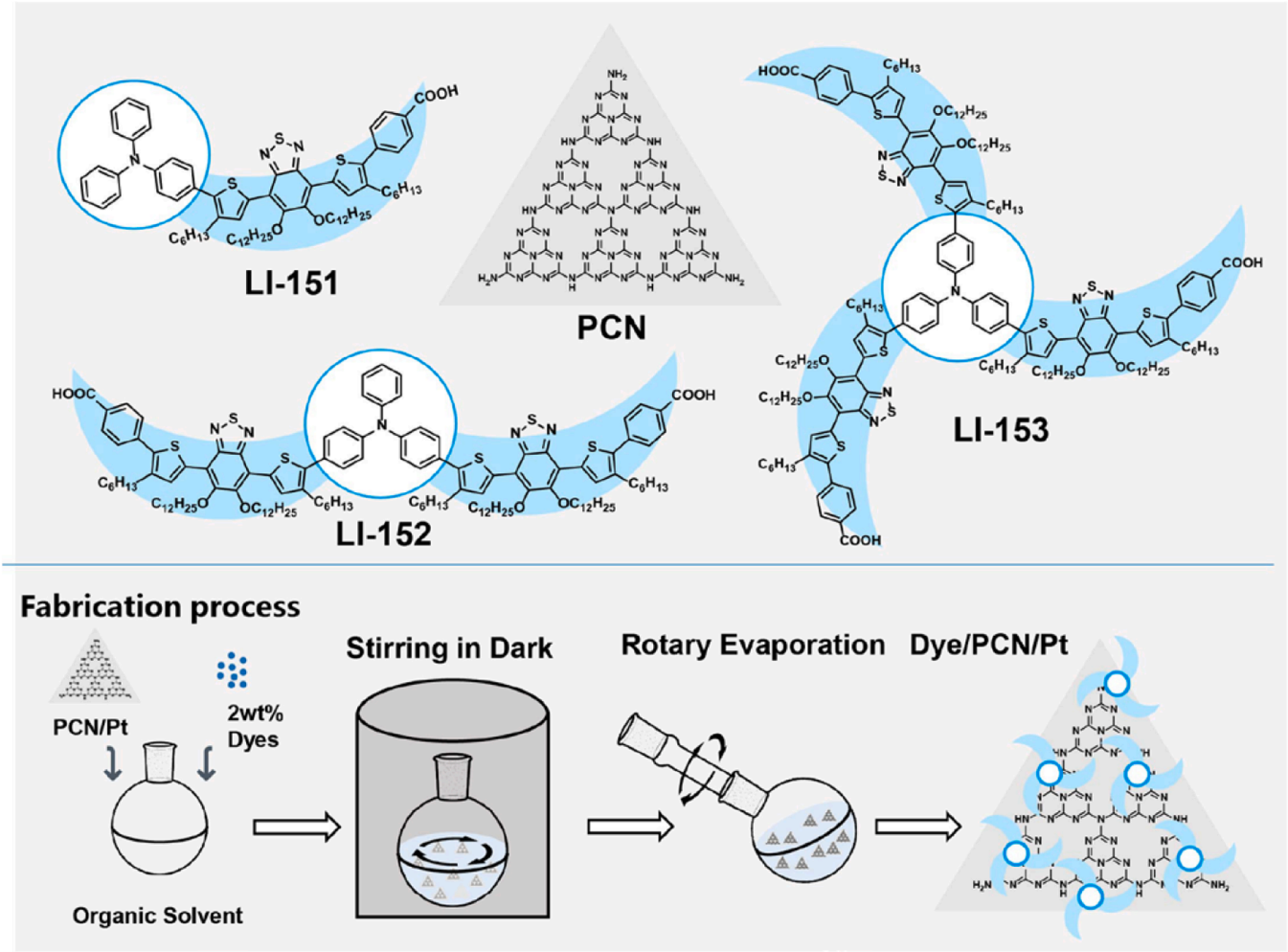

Scheme 1. Molecular structures of dye **LI-151**, **LI-152**, **LI-153** and PCN, and schematically illustration of fabrication processes of dye/PCN/Pt photocatalytic systems.

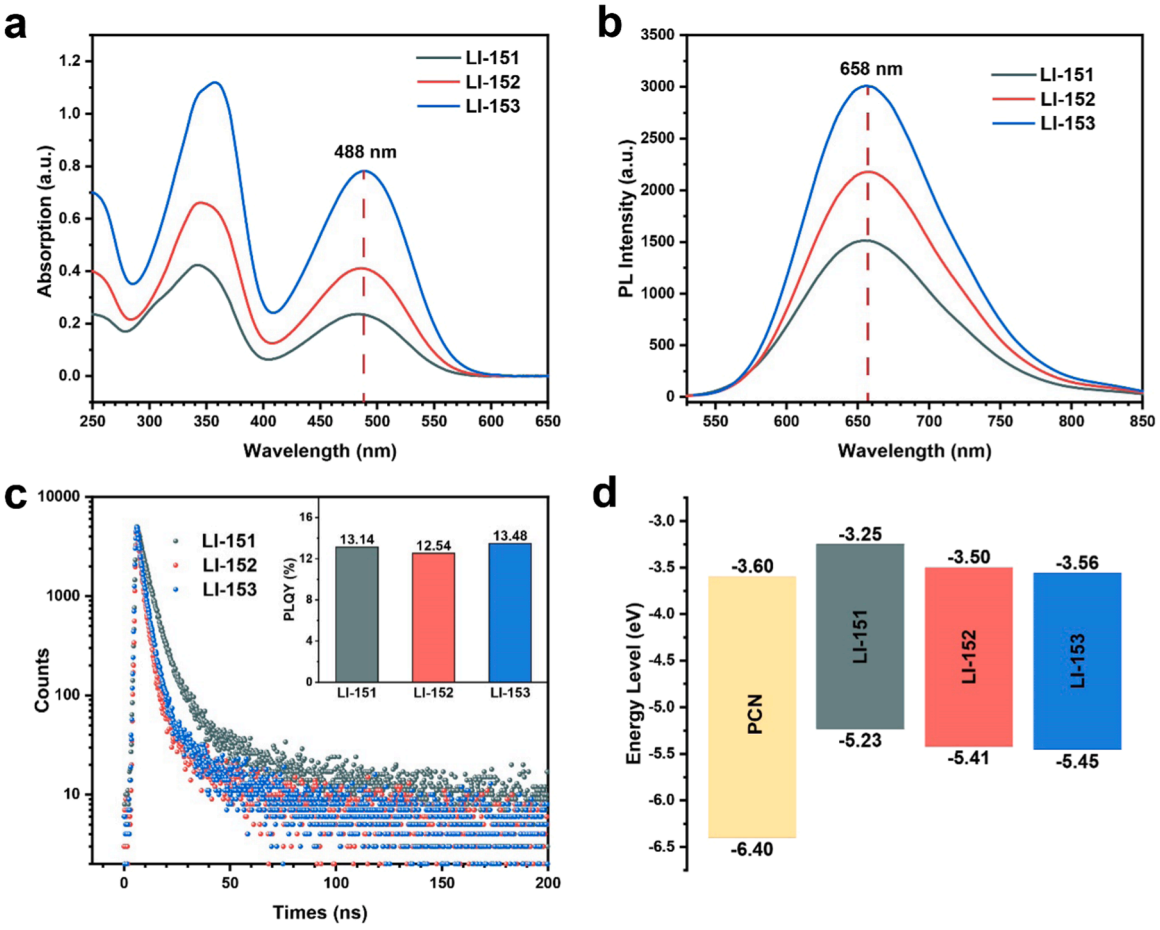

Fig. 1. a) UV–vis absorption spectra of dyes **LI-151**, **LI-152** and **LI-153** in dilute solution ($CHCl_3/CH_3OH$ (4:1), 1×10^{-5} mol L^{-1}) b) PL spectra of dyes **LI-151**, **LI-152** and **LI-153** in dilute solution ($CHCl_3/CH_3OH$ (4:1), 1×10^{-5} mol L^{-1}) by excitation at 515 nm. c) PL decay (solid state, $\lambda_{ex} = 450$ nm, $\lambda_{em} = 650$ nm) and PLQY in dilute solution ($CHCl_3/CH_3OH$ (4:1), 1×10^{-5} mol L^{-1}) of **LI-151**, **LI-152** and **LI-153** (Rhodamine B as a standard reference). d) Energy diagram of PCN, **LI-151**, **LI-152** and **LI-153**.

Table 1
Photophysical properties of dye **LI-151**, **LI-152** and **LI-153**.

Dye	λ_{abs} [a]	λ_{onset} [a]	λ_{onset} [b]	λ_{em} [c]	λ_{em} [d]	ε [e] × 10^4	Φ [f]	τ_{ave} [g]	E_{0-0} [h]	E_{HOMO} [i]	E_{LUMO} [j]
	[nm]	[nm]	[nm]	[nm]	[nm]	[mol L^{-1} cm^{-1}]	[%]	[ns]	[eV]	[eV]	[eV]
LI-151	342, 482	560	649	656	652	2.62	13.14	6.26	1.98	-5.23	-3.25
LI-152	345, 486	561	666	658	671	4.80	12.54	4.58	1.91	-5.41	-3.50
LI-153	357, 489	563	682	658	678	6.98	13.48	4.76	1.89	-5.45	-3.56

[a] The UV–vis absorption spectra of dyes in $CHCl_3/CH_3OH$ (4:1) solution at the concentration of 1×10^{-5} mol L^{-1}.
[b] UV–vis DRS absorption spectra of dyes (solid state).
[c] The PL spectra of dyes in $CHCl_3/CH_3OH$ (4:1) solution at the concentration of 1×10^{-5} mol L^{-1}.
[d] The PL spectra of organic dyes at solid state.
[e] Molar extinction coefficient of dyes in $CHCl_3/CH_3OH$ (4:1) solution.
[f] Photoluminescence quantum yield of dyes in $CHCl_3/CH_3OH$ (4:1) solution.
[g] PL lifetimes of dyes at solid state.
[h] The optical band gap of dyes as measured by Tauc-plots.
[i] HOMO energy levels as calculated by UPS.
[j] LUMO energy levels as calculated by $E_{LUMO} = E_{HOMO} - E_{0-0}$.

photoluminescence (PL) intensities can be observed by the increased number of branched structures. The brightest photoluminescence property is achieved by **LI-153** with octupolar structure, which may be related to the cooperative effect by the three branches with well-organized geometry. Also, **LI-153** exhibited the slightly higher photoluminescence quantum yield (PLQY) of 13.48% (Fig. 1c, Table 1), meaning the less nonradiative transitions in the multibranched structure. It can benefit to PHE process for suppression of energy loss. The lifetimes of **LI-151**, **LI-152** and **LI-153** are calculated to be 6.26 ns, 4.58 ns and 4.76 ns, respectively. With the increased concentrations of these organic dyes, nearly no aggregation caused quenching (ACQ) effect can be observed (Fig. S14). Alternatively, aggregation-induced

emission (AIE) effect is obvious upon the addition of water into organic solvent gradually (Fig. S15), and the highest PL intensity is achieved by **LI-153**, suggesting the optimized molecular aggregates by three-branched structures. Once these molecules aggregated into solid states, the red-shifted absorption is obvious with the onset wavelength extended to ~700 nm (Fig. S16), further favoring to the light harvesting for photocatalytic process. Accordingly, the PL spectra of three organic dyes exhibited different shifts, compared to those in solution, which is possibly related to varied aggregated structures by their different geometries (Fig. S17). The optical bandgaps of **LI-151**, **LI-152** and **LI-153** are 1.98 eV, 1.91 eV and 1.89 eV, respectively (Fig. S18), and the decreased values with the increased number of branched structures may cause by the possible electronic coupling among branched moieties. Their HOMO and LUMO energy levels (Fig. 1d, Fig. S19) are well-matched with PCN (Fig. S19, Fig. S24), suggesting the successful heterojunction systems with efficient charge transfer processes.

These energy levels are determined by molecular configurations and electronic properties of organic dyes, which can be illustrated by theory calculation with Gaussian 09 program at B3LYP/6–31 G(D) [43]. With the increased number of branches, the optimized molecular configurations of dye **LI-151**, **LI-152** and **LI-153** are rod-like, V-shape, and trigonal pyramidal geometries, respectively. The same branched structure in three dyes exhibited the almost planar configuration, and the dihedral angles between adjacent moieties are in the range of 6–40° (Fig. S20). This is mainly related to the possible O…S interactions between thiophene and the adjacent alkoxy groups as the side substituents to benzothiazole unit. It can be further confirmed by the large rotation energy barrier of C-C bond between thiophene and benzothiazole moieties in **LI-151** (Fig. S21), the varied molecular energies with the tuable thiophene orientations and the presence of the alkoxyl chains or not (Fig. S22). Accordingly, the well-overlaps of HOMO and LUMO distributions can be observed, in which, HOMOs are mainly located at the TPA and thiophene moieties, and LUMOs are mainly distributed at benzothiazole and thiophene moieties in different branches. It can benefit to light harvesting and carrier transporting for the efficient charge transfer from the TPA core (D) to benzothiazole (A) in the each branch.

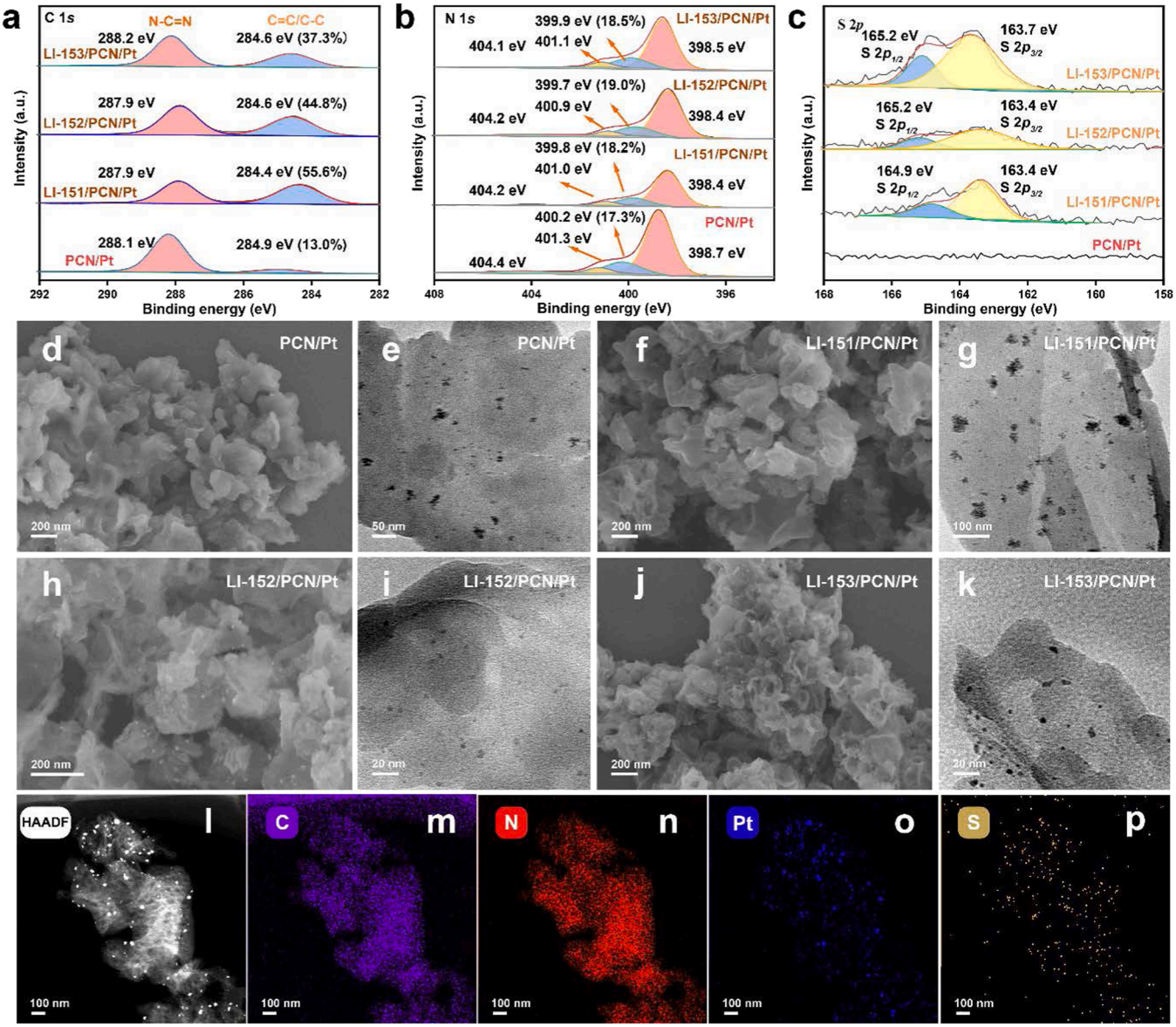

Fig. 2. High-resolution XPS spectra of PCN/Pt and dye/PCN/Pt: a) C 1 s, b) N 1 s, and c) S 2p. d–k) SEM and TEM images of PCN/Pt (d, e) and LI-151/PCN/Pt (f, g), LI-152/PCN/Pt (h, i), LI-153/PCN/Pt (j, k). l) HAADF-STEM image of LI-153/PCN/Pt. m–p) Elemental mapping images of LI-153/PCN/Pt with elemental distribution of m) C, n) N, o) Pt and p) S.

3.2. Dye/PCN/ Pt heterojunction systems

Subsquently, in order to fabricate the heterojunction systems, $CHCl_3$ and MeOH are chosen as the solvents for their good solubility for organic dyes. Firstly, PCN/Pt system was formed by the photo-deposition of Pt on the surface of PCN. After the dye (2 wt%) and PCN/Pt were fully mixed in solution, the organic solvent were removed by rotary evaporators to yield the dye/PCN/Pt system (Scheme 1, see detail in Supproting information). The XRD pattern of dye/PCN/Pt is similar to that of PCN/Pt (XRD, Fig. S25), and the characteristic pattern of Pt is consistent with the data in the spectral library, indicating that the addition of organic dyes does not break the optimized aggregated state of PCN/Pt.

Furthermore, X-ray photoelectron spectroscopy (XPS) are performed to identify surface information of the prepared photocatalysts. As shown in Fig. 2a, the high-resolution C 1 s spectra of PCN/Pt and dye/PCN/Pt systems can be resolved into two major peaks at about 288 eV and about 284 eV, which can be indexed as N-C═N and C═C/C-C bonds, respectively [53,54]. Compared to PCN/Pt system, the ratio of peak at about 284 eV in dye/PCN/Pt increased significantly for the additional aromatic moieties in these dyes. Accordingly, two characteristic peaks in the high-resolution S 2p XPS spectra of dye/PCN/Pt at about 163 eV and about 165 eV (Fig. 2c) are corresponded to S $2p_{1/2}$ and S $2p_{3/2}$, respectively, which are from the benzothiazole moieties of organic dyes [29,55].

In the high-resolution N 1 s spectra (Fig. 2b), the four peaks of PCN/Pt can be assigned to π excitations (about 404 eV), quaternary N (C-NH) (about 401 eV), tertiary N (N-$(C)_3$) (about 400 eV) and sp^2-hybridized aromatic N (C═N-C) (about 398 eV), respectively [56]. Compared to PCN/Pt, the increased ratios of dye/PCN/Pt at about 400 eV are assigned to C-N bonds in TPA unit of organic dyes. Meanwhile, the slightly lower binding energies of dye/PCN/Pt than that of PCN/Pt (Table S2), suggests the increased electron density of N atom after the incorporation of organic dyes, which is mainly related to the possible charge transfer process from organic dyes to PCN through intermolecular π-π interactions (Fig. 2b) [30,57].

Scanning electron microscope (SEM) and transmission electron microscope (TEM) image clarify that the lamellar morphologies of PCN are not damaged during the preparation of photocatalyst PCN/Pt (Fig. S26). The deposited Pt particles are uniformly distributed on the surface of PCN as small particles (Fig. S27), and no specific structure of dyes was observed in the dye/PCN/Pt sample for the low concentration (2 wt%). However, it can be observed in the elemental mapping images with LI-153/PCN/Pt system as an example (Fig. 2l-p). The brightest point in

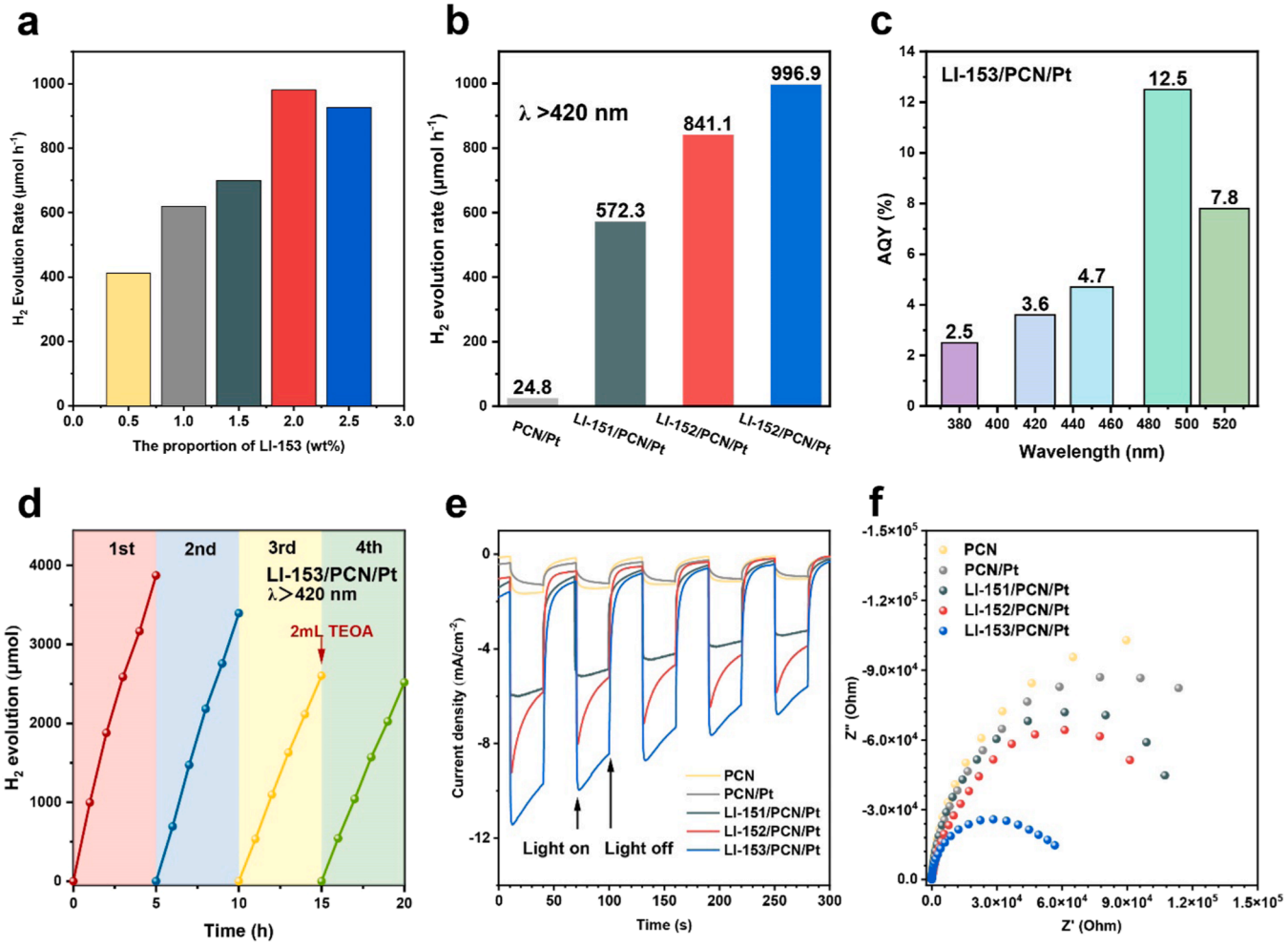

Fig. 3. a) The photocatalytic hydrogen evolution activities of LI-153/PCN/Pt systems with the different proportion of dyes under visible-light irradiation (50 mg photocatalyst, 10 mL TEOA, 100 mL H_2O, 300 W Xe lamp with cut-off filter λ ≥ 420 nm). b) The photocatalytic hydrogen evolution activities of PCN/Pt and dye/PCN/Pt systems under visible-light irradiation (50 mg photocatalyst, 10 mL TEOA, 100 mL H_2O, 300 W Xe lamp with cut-off filter λ ≥ 420 nm). c) Calculated AQY of LI-153/PCN/Pt under illumination with different wavelengths. d) Cycling measurements of LI-153/PCN/Pt under visible-light irradiation (50 mg photocatalyst, 10 mL TEOA, 100 mL H_2O, 300 W Xe lamp with cut-off filter λ ≥ 420 nm). e) Transient photocurrent densities of PCN, PCN/Pt and dye/PCN/Pt electrodes in 0.5 M Na_2SO_4 solution under the irradiation of visible light (λ ≥ 420 nm). f) Electrochemical impedance spectra (EIS) of PCN, PCN/Pt and dye/PCN/Pt in 0.5 M Na_2SO_4 solution under the irradiation of visible light (λ ≥ 420 nm) (Nyquist plots).

the HAADF-STEM picture (Fig. 2l) corresponded to Pt with the biggest atomic number among C, N, O and S elements, which is consistent with the distribution of Pt in Fig. 2o. The part with slightly weaker brightness than that of Pt, corresponded to the S element in benzothiazole moiety, indicating the well-dispersion of **LI-153** on the surface of PCN. It can be further confirmed by the distribution diagram of S element in Fig. 2p. The light-harvesting of dye/PCN/Pt system in the visible region is mainly from the doped organic dyes, even in low concentrations, as confirmed by the absent absorption of PCN/Pt in the region of 450–600 nm (Fig. S23). It can promote the photocatalytic hydrogen evolution for the extended light-harvesting region (300–600 nm). Also, compared to bare PCN, the VB XPS of dye/PCN/Pt showed slightly offset (Fig. S28).

3.3. Photocatalytic hydrogen production and stability

The photocatalytic activities of dye/PCN/Pt systems were evaluated with triethanolamine (TEOA) as sacrificial agent under light irradiation ($\lambda \geq 420$ nm). With the aim to determine the preferred concentration of organic dyes to hydrogen production, PHE activities of LI-153/PCN/Pt systems with the different amount of dyes have been measured. As shown in Fig. 3a, with the increased proportion of dye from 0.5% to 2.5% (wt%), the PHE rate of LI-153/PCN/Pt system firstly increased, then decreased. The maximum value was achieved at the dye content of 2.0%, indicating it is the optimal ratio for water splitting. Thus, the follwing experiments of PHE systems were conducted with the fixed concentration (2.0%) of organic dyes. As shown in Fig. 3b, the PCN/Pt exhibited low H_2 generation activity with the rate of 24.8 μmol h^{-1}. After the incorporation of organic dyes by the simple doping process, the PHE performance enhanced with the increased number of branched structures. LI-153/PCN/Pt exhibited the highest PHE rate of 996.9 μmol h^{-1} under visible-light irradiation, about 43-foldes enhancement of that of PCN/Pt. It is speculated that dye **LI-153** with three-branched structure may result in the well distribution on the surface of PCN/Pt, which can promote the charge transfer processes at the interface, and then improve the PHE performance. Furthermore, the apparent quantum yields (AQYs) of LI-153/PCN/Pt (Fig. 3c, Table S4) are over 2.5% in the broad region of 380–520 nm, which reaches to the highest one of 12.5% at 490 nm. Compared to PCN with AQYs of 1.2% and 1.0% at only 420 nm and 380 nm (Table S3), respectively, LI-153/PCN/Pt shows greatly improvement in the conversion of incident photos into hydrogen by the extended light harvesting region and the efficient charge transfer processes. Besides, the good photochemical stability has been proved by the ignorable variation of absorption spectra of the thin film under the continuous sunlight irradiation of 25 h (Fig. S29), and four cycles of the photocatalysis reaction were examined. The PHE performance of LI-153/PCN/Pt decreased from 996.9 μmol h^{-1} (first cycle) to 533.4 μmol h^{-1} in third cycles (Fig. 3d), and no further decrease of the fourth cycle is observed after TEOA supplementation. Since the structure of PCN is not damaged during the longtime irradiation, as proved by FTIR (Fig. S30), UV–vis DRS (Fig. S31) and XRD (Fig. S32), the dye degradation and the enlarged size of Pt particle may be the main reason to the decreased PHE activity [22].

3.4. Investigations of charge transfer processes

The charge transfer processes are investigated by photoelectrochemical measurements. As shown in Fig. 3e, all the dye/PCN/Pt electrodes display higher transient photocurrent response than that of PCN/Pt, and LI-153/PCN/Pt behaves the highest intensity, meaning the most efficient charge separation. Electrochemical impedance spectroscopy (EIS) under light irradiation is shown in Fig. 3f, and the smaller semi-circular curve in Nyquist plots represents the less charge transfer resistance. Obviously, the lowest charge transfer resistance in LI-153/PCN/Pt proves the most efficient charge transfer processes, which is consisted with the excellent PHE performance of LI-153/PCN/Pt.

These charge transfer processes are highly related to the formation of efficient heterojunction system, which can be further confirmed by the PL spectra under different fabrication processes. One is dye/PCN/Pt system as mentioned above, the other one was fabricated by adding PCN/Pt to the dye solution with the same mass concentration (2 wt%) directly, named as dye+PCN/Pt, in which the interactions between dye and PCN can be ignored for the low concentration of solution (0.02 mg mL^{-1}). PL intensities of the two samples were measured in organic solvent ($CHCl_3/CH_3OH$ (4:1))/aqueous (H_2O/TEOA (10:1)) mixtures with different aqueous fractions (10–90%, Fig. S33-S38). The PL intensity of dye/PCN/Pt system at 650 nm is obviously lower than that of dye+PCN/Pt, whether under the excitation of visible (560 nm) or ultraviolet light (350 nm), indicating the existence of charge transfer process in heterojunction system, as the energy loss for radiative transitions under different conditions.

With the aim to further reveal the effect of the branch structures on the binding modes between dyes and PCN, the surface information of photocatalysts was investigated by their water contact angles. The originally hydrophilic PCN/Pt electrodes (Fig. 4a) turned to hydrophobic ones, after being loaded with **LI-151**, **LI-152** and **LI-153** (Fig. 4b-d). With the increased branch degrees of organic dyes, the water contact angles increased gradually from 119.0° (**LI-151**), to 125.7° (**LI-152**), then to 137.2° (**LI-153**). Also, LI-153/PCN/Pt presented lower Brunauer—Emmett–Telle (BET) surface area, compared to those of PCN and PCN/Pt, as calculated from the nitrogen adsorption isotherms measured at 77 K (Fig. 4e). It may be related to the possible insertion of **LI-153** into the pores of PCN, as well as the covering effect on the surface. Moreover, the multiple carboxyl groups in dye **LI-153** can be used as the anchoring groups to PCN, presenting a claw-like function on the surface. Thus, dye **LI-153** with three-branched structure may cover the defects on the surface of PCN effectively, resulting in the improved charge transfer between dye and PCN.

The efficient charge transfer possess can be further investigated by PL spectra and decay (Fig. S39-S40). With the emission peak of PCN at 450 nm as the object, the incorporation of Pt and/or organic dyes can decrease the emission intensity largely for the efficient charge transfer at the dye/PCN/Pt interface, accompanying with the decreased lifetimes from 9.47 ns to 7.74 ns [58,59]. The sharp decrease of LI-153/PCN/Pt with the shortest lifetime (7.74 ns) means the most efficient charge transfer, which is mainly related to the multi-branched structures with more channels. Alternatively, with the emission peak of organic dyes at 650 nm as the object, the decreased intensities with the incorporation of PCN and Pt are obvious, further confirming the efficient charge transfer inside photocatalysis. Accordingly, the most efficient charge transfer by the incorporation of **LI-153** is further confirmed, in good agreement of excellent PHE performance of LI-153/PCN/Pt system.

4. Conclusions

In summary, three organic dyes with different number of branched structures are synthesized and applied to PCN surface as the light-harvesting and charge transporting materials. With the increased numbers of branches bearing electronic pull-push property, the PHE performance enhanced gradually. The highest one (996.9 μmol h^{-1}) is achieved by dye **LI-153** with three branches, over 40-foldes that of bare PCN (24.8 μmol h^{-1}), indicating the advantage of multiple branched structures. They can afford the multi-channels for charge transfer, and suppress the possible energy loss by the well-organized geometry of branches. Also, the trigonal pyramidal geometry with three anchoring units can be beneficail to the interactions between dyes and PCN, as confirmed by the variations of PL intensities under different conditions, EIS spectra, BET surface areas and water contact angles. Thus, some relationship between hydrogen evolution and molecular geometry has been proposed: (1) the multiple branched structure can suppress the possible molecular aggregates of organic dyes with high polarity, favoring to the efficient charge transfer process at the interface; (2) the

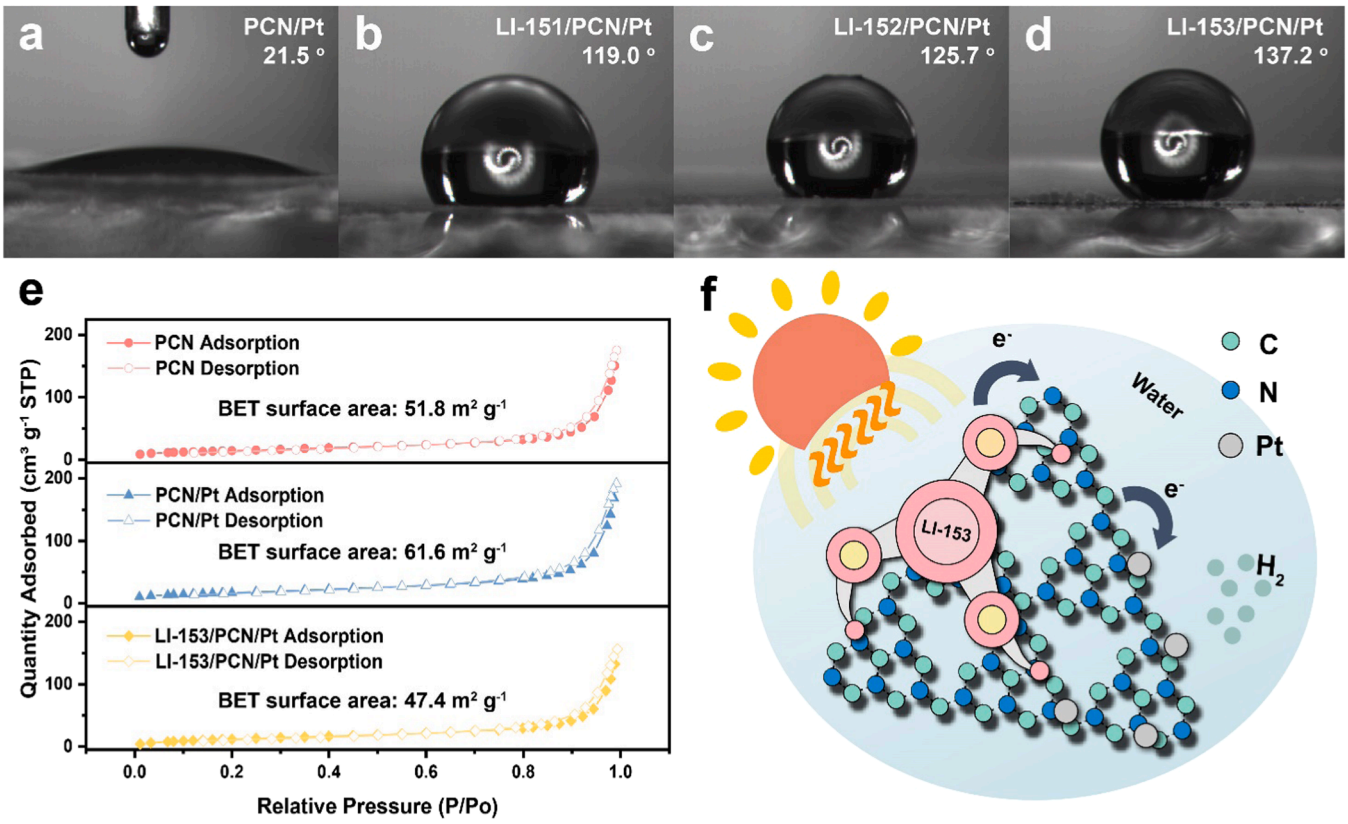

Fig. 4. The water contact angles of a) PCN/Pt, b) LI-151/PCN/Pt, c) LI-152/PCN/Pt and d) LI-153/PCN/Pt electrodes. e) Nitrogen adsorption-desorption isotherms of PCN, PCN/Pt and LI-153/PCN/Pt. f) Schematic diagram of the charge transfer processes between **LI-153** and PCN.

propeller-like geometries with multiple ICT process can improve the light-harvesting property. Our findings provide a desirable way to promote the photocatalytic hydrogen evolution by the rational design of organic dyes, and the function of multiple-branched molecular structure is highlighted.

CRediT authorship contribution statement

Qianqian Li and Zhen Li conceived the project. Siwei Liu synthesized the organic compounds and performed all the measurements. Peixuan Lin performed part of the synthetic experiments and photoelectrochemical measurements. Meng Wu and Zhi-An Lan performed part of photocatalytic test. Hangyu Zhuzhang helped to synthesize the polymeric carbon nitride. Mengmeng Han performed the DFT calculations. Yunhao Fan conducted the photoluminescence spectra and lifetimes. Xiong Chen and Xinchen Wang afforded the platform for photocatalytic test. Qianqian Li and Zhen Li discussed and revised the manuscript. All the authors approved the manuscript.

Declaration of Competing Interest

The authors declare that they have no known competing financial interests or personal relationships that could have appeared to influence the work reported in this paper.

Acknowledgments

We are grateful to the National Natural Science Foundation of China (no. 21875174, 21734007), and Excellent Youth Foundation of Hubei Scientific Committee (2020CFA084), the Fundamental Research Funds for the Central Universities (2042021kf1073) and Wuhan City (2019010701011412) for financial support. The authors would like to acknowledge the Center for Electron Microscopy at Wuhan University for their substantial supports to TEM work.

Appendix A. Supporting information

Supplementary data associated with this article can be found in the online version at doi:10.1016/j.apcatb.2022.121257.

References

[1] Y. Fang, Y. Zheng, T. Fang, Y. Chen, Y. Zhu, Q. Liang, H. Sheng, Z. Li, C. Chen, X. Wang, Photocatalysis: an overview of recent developments and technological advancements, Sci. China Chem. 63 (2020) 149–181.
[2] T. Hisatomi, J. Kubota, K. Domen, Recent advances in semiconductors for photocatalytic and photoelectrochemical water splitting, Chem. Soc. Rev. 43 (2014) 7520–7535.
[3] S. Chen, T. Takata, K. Domen, Particulate photocatalysts for overall water splitting, Nat. Rev. Mater. 2 (2017) 17050.
[4] X. Chen, S. Shen, L. Guo, S.S. Mao, Semiconductor-based photocatalytic hydrogen generation, Chem. Rev. 110 (2010) 6503–6570.
[5] S. Chen, Y. Qi, T. Hisatomi, Q. Ding, T. Asai, Z. Li, S.S.K. Ma, F. Zhang, K. Domen, C. Li, Efficient visible-light-driven z-scheme overall water splitting using a MgTa2O6−xNy/TaON heterostructure photocatalyst for H2 evolution, Angew. Chem. 127 (2015) 8618–8621.
[6] J. Hou, B. Zhang, Z. Li, S. Cao, Y. Sun, Y. Wu, Z. Gao, L. Sun, Vertically Aligned Oxygenated-CoS2–MoS2Heteronanosheet Architecture from Polyoxometalate for Efficient and Stable Overall Water Splitting, ACS Catal. 8 (2018) 4612–4621.
[7] B. Dong, J. Cui, Y. Gao, Y. Qi, F. Zhang, C. Li, Heterostructure of 1D Ta3N5Nanorod/BaTaO2N Nanoparticle Fabricated by a One-Step Ammonia Thermal Route for Remarkably Promoted Solar Hydrogen Production, Adv. Mater. 31 (2019), 1808185.
[8] J. Hou, H. Cheng, O. Takeda, H. Zhu, Unique 3D heterojunction photoanode design to harness charge transfer for efficient and stable photoelectrochemical water splitting, Energy Environ. Sci. 8 (2015) 1348–1357.
[9] X. Wang, K. Maeda, A. Thomas, K. Takanabe, G. Xin, J. Carlsson, K. Domen, M. Antonietti, A metal-free polymeric photocatalyst for hydrogen production from water under visible light, Nat. Mater. 8 (2009) 76–80.

[10] Y. Wang, X. Wang, M. Antonietti, Polymeric graphitic carbon nitride as a heterogeneous organocatalyst: from photochemistry to multipurpose catalysis to sustainable chemistry, Angew. Chem. Int. Ed. 51 (2012) 68–89.
[11] Y. Wang, A. Vogel, M. Sachs, R.S. Sprick, L. Wilbraham, S.J.A. Moniz, R. Godin, M. A. Zwijnenburg, J.R. Durrant, A.I. Cooper, J. Tang, Current understanding and challenges of solar-driven hydrogen generation using polymeric photocatalysts, Nat. Energy 4 (2019) 746–760.
[12] J. Zhang, X. Chen, K. Takanabe, K. Maeda, K. Domen, J.D. Epping, X. Fu, M. Antonietti, X. Wang, Synthesis of a carbon nitride structure for visible-light catalysis by copolymerization, Angew. Chem. Int. Ed. 49 (2010) 441–444.
[13] W.-J. Ong, L.-L. Tan, Y.H. Ng, S.-T. Yong, S.-P. Chai, Graphitic Carbon Nitride (g-C3N4)-Based Photocatalysts for Artificial Photosynthesis and Environmental Remediation: Are We a Step Closer To Achieving Sustainability? Chem. Rev. 116 (2016) 7159–7329.
[14] H. Cai, B. Wang, L. Xiong, J. Bi, L. Yuan, G. Yang, S. Yang, Orienting the charge transfer path of type-II heterojunction for photocatalytic hydrogen evolution, Appl. Catal. B 256 (2019), 117853.
[15] K. Li, W.-D. Zhang, Creating Graphitic Carbon Nitride Based Donor-π-Acceptor-π-Donor Structured Catalysts for Highly Photocatalytic Hydrogen Evolution, Small 14 (2018), 1703599.
[16] Z. Pan, M. Liu, G. Zhang, H. Zhuzhang, X. Wang, Molecular triazine–heptazine junctions promoting exciton dissociation for overall water splitting with visible light, J. Phys. Chem. C. 125 (2021) 9818–9826.
[17] B. Zhu, B. Cheng, J. Fan, W. Ho, J. Yu, g-C3N4-based 2D/2D composite heterojunction photocatalyst, Small Struct. 2 (2021), 2100086.
[18] Q. Zhu, Z. Xu, B. Qiu, M. Xing, J. Zhang, Emerging Cocatalysts on g-C3N4for Photocatalytic Hydrogen Evolution, Small 17 (2021), 2101070.
[19] Y. Xiao, Y. Qi, X. Wang, X. Wang, F. Zhang, C. Li, Visible-Light-Responsive 2D Cadmium-Organic Framework Single Crystals with Dual Functions of Water Reduction and Oxidation, Adv. Mater. 30 (2018), 1803401.
[20] C. Ru, Q. Wei, W. Chen, Q. Guan, Q. Zhang, Y. Ling, C. Tao, D. Qin, J. Wu, X. Pan, Tunable Conjugated Organoborane Oligomers for Visible-Light-Driven Hydrogen Evolution, ACS Energy Lett. 5 (2020) 669–675.
[21] Y. Si, Z. Lv, L. Lu, M. Liu, Y. Wen, Y. Chen, H. Jin, J. Liu, W. Song, Revealing important role of graphitic carbon nitride surface catalytic activity in photocatalytic hydrogen evolution by using different carbon co-catalysts, Appl. Surf. Sci. 491 (2019) 236–244.
[22] F. Su, S.C. Mathew, G. Lipner, X. Fu, M. Antonietti, S. Blechert, X. Wang, mpg-C(3)N(4)-Catalyzed selective oxidation of alcohols using O(2) and visible light, J. Am. Chem. Soc. 132 (2010) 16299–16301.
[23] J.Y. Bai, L.J. Wang, Y.J. Zhang, C.F. Wen, X.L. Wang, H.G. Yang, Carboxyl functionalized graphite carbon nitride for remarkably enhanced photocatalytic hydrogen evolution, Appl. Catal. B 266 (2020), 118590.
[24] Y. Li, R. He, P. Han, B. Hou, S. Peng, C. Ouyang, A new concept: Volume photocatalysis for efficient H2 generation _ Using low polymeric carbon nitride as an example, Appl. Catal. B 279 (2020), 119379.
[25] Q. Yang, M. Luo, K. Liu, H. Cao, H. Yan, Covalent organic frameworks for photocatalytic applications, Appl. Catal. B 276 (2020), 119174.
[26] X. Zhang, T. Peng, S. Song, Recent advances in dye-sensitized semiconductor systems for photocatalytic hydrogen production, J. Mater. Chem. A 4 (2016) 2365–2402.
[27] H. Ding, M. Xu, S. Zhang, F. Yu, K. Kong, Z. Shen, J. Hua, Organic blue-colored D-A-π-A dye-sensitized TiO2 for efficient and stable photocatalytic hydrogen evolution under visible/near-infrared-light irradiation, Renew. Energ. 155 (2020) 1051–1059.
[28] S. Min, G. Lu, Enhanced Electron Transfer from the Excited Eosin Y to mpg-C3N4for Highly Efficient Hydrogen Evolution under 550 nm Irradiation, J. Phys. Chem. C. 116 (2012) 19644–19652.
[29] F. Yu, Z. Wang, S. Zhang, K. Yun, H. Ye, X. Gong, J. Hua, H. Tian, N-Annulated perylene-based organic dyes sensitized graphitic carbon nitride to form an amide bond for efficient photocatalytic hydrogen production under visible-light irradiation, Appl. Catal. B 237 (2018) 32–42.
[30] K. Li, L. Wang, Z. Chen, X. Yang, Y.-X. Yu, W.-D. Zhang, Y. Wang, Y. Shi, K.P. Loh, Q.-H. Xu, Photocatalytic hydrogen evolution under ambient conditions on polymeric carbon nitride/donor-π-acceptor organic molecule heterostructures, Adv. Funct. Mater. 30 (2020), 2005106.
[31] S. Wang, X. Xu, Y. Yue, K. Yu, Q. Shui, N. Huang, H. Chen, Semiconductive covalent organic frameworks: structural design, synthesis, and application, Small Struct. 1 (2020), 2000021.
[32] J. Wang, S. Liu, Z. Chai, K. Chang, M. Fang, M. Han, Y. Wang, S. Li, H. Han, Q. Li, Z. Li, Significantly improved performance of dye-sensitized solar cells by optimizing organic dyes with pyrrole as the isolation spacer and utilizing alkyl chain engineering, J. Mater. Chem. A 6 (2018) 22256–22265.
[33] H. Li, Y. Yang, Y. Hou, R. Tang, T. Duan, J. Chen, H. Wang, H. Han, T. Peng, X. Chen, Q. Li, Z. Li, Organic Sensitizers Featuring 9,10-Diaryl-Substituted Anthracene Unit, ACS Sustain. Chem. Eng. 2 (2014) 1776–1784.
[34] Z. Chai, M. Wu, M. Fang, S. Wan, T. Xu, R. Tang, Y. Xie, A. Mei, H. Han, Q. Li, Z. Li, Similar or totally different: the adjustment of the twist conformation through minor structural modification, and dramatically improved performance for dye-sensitized solar cell, Adv. Energy Mater. 5 (2015), 1500846.
[35] S. Wang, X. Hai, X. Ding, S. Jin, Y. Xiang, P. Wang, B. Jiang, F. Ichihara, M. Oshikiri, X. Meng, Y. Li, W. Matsuda, J. Ma, S. Seki, X. Wang, H. Huang, Y. Wada, H. Chen, J. Ye, Intermolecular cascaded π-conjugation channels for electron delivery powering CO_2 photoreduction, Nat. Commun. 11 (2020) 1149.
[36] C. Yang, B.C. Ma, L. Zhang, S. Lin, S. Ghasimi, K. Landfester, K.A. Zhang, X. Wang, Molecular Engineering of Conjugated Polybenzothiadiazoles for Enhanced Hydrogen Production by Photosynthesis, Angew. Chem. Int. Ed. 55 (2016) 9202–9206.
[37] Z.-A. Lan, M. Wu, Z. Fang, X. Chi, X. Chen, Y. Zhang, X. Wang, A fully coplanar donor-acceptor polymeric semiconductor with promoted charge separation kinetics for photochemistry, Angew. Chem. Int. Ed. 60 (2021) 16355–16359.
[38] G. Li, Z. Xie, Q. Wang, X. Chen, Y. Zhang, X. Wang, Asymmetric acceptor-donor-acceptor polymers with fast charge carrier transfer for solar hydrogen production, Chem. Eur. J. 27 (2021) 939–943.
[39] H. Li, Y. Yang, R. Tang, J. Chen, H. Wang, H. Han, T. Peng, Q. Li, Z. Li, Attempt to improve the performance of pyrrole-containing dyes in dye sensitized solar cells by adjusting isolation groups, ACS Appl. Mater. Interfaces 5 (2013) 12469–12477.
[40] W. Wu, Z. Xu, Z. Li, Using low generation dendrimers as monomers to construct dendronized hyperbranched polymers with high nonlinear optical performance, J. Mater. Chem. C. 2 (2014) 8122–8130.
[41] W. Wu, Z. Li, Further improvement of the macroscopic NLO coefficient and optical transparency of hyperbranched polymers by enhancing the degree of branching, Polym. Chem. 5 (2014) 5100–5108.
[42] W. Wu, Y. Fu, C. Wang, Z. Xu, C. Ye, J. Qin, Z. Li, Second-order nonlinear optical hyperbranched polymer containing isolation chromophore moieties derived from both "H"-type and star-type chromophores, Chin. J. Polym. Sci. 31 (2013) 1415–1423.
[43] Z.-A. Lan, Y. Fang, Y. Zhang, X. Wang, Photocatalytic oxygen evolution from functional triazine-based polymers with tunable band structures, Angew. Chem. Int. Ed. 57 (2018) 470–474.
[44] Q. Li, J. Zou, J. Chen, Z. Liu, J. Qin, Z. Li, Y. Cao, New indole-based light-emitting oligomers: structural modification, photophysical behavior, and electroluminescent properties, J. Phys. Chem. B 113 (2009) 5816–5822.
[45] Q. Li, J. Huang, A. Zhong, C. Zhong, M. Peng, J. Liu, Z. Pei, Z. Huang, J. Qin, Z. Li, N-arylpyrrole-based chromophores of donor-π-donor type displaying high two-photon absorption, J. Phys. Chem. B 115 (2011) 4279–4285.
[46] J. Fu, Z. Mo, M. Cheng, F. X, Y. Song, X. Ding, Z. Chen, H. Chen, H. Li, H. Xu, An all-organic TPA-3CN/2D-C3N4 heterostructure for high efficiency photocatalytic hydrogen evolution, Colloids Surf. A Physicochem. Eng. Asp. 589 (2020), 124397.
[47] S.K. Choi, H.S. Yang, J.H. Kim, H. Park, Organic dye-sensitized TiO2 as a versatile photocatalyst for solar hydrogen and environmental remediation, Appl. Catal. B. 121–122 (2012) 206–213.
[48] D. Gudeika, A. Michaleviciute, J.V. Grazulevicius, R. Lygaitis, S. Grigalevicius, V. Jankauskas, A. Miasojedovas, S. Jursenas, G. Sini, Structure properties relationship of donor–acceptor derivatives of triphenylamine and 1,8-naphthalimide, J. Phys. Chem. C. 116 (2012) 14811–14819.
[49] W. Wu, R. Tang, Q. Li, Z. Li, Functional hyperbranched polymers with advanced optical, electrical and magnetic properties, Chem. Soc. Rev. 44 (2015) 3997–4022.
[50] C.-F. Liu, Y. Jiu, J. Wang, J. Yi, X.-W. Zhang, W.-Y. Lai, W. Huang, Gene silencing of USP1 by lentivirus effectively inhibits proliferation and invasion of human osteosarcoma cells, Macromolecules 49 (2016) 2549–2557.
[51] Z.-A. Lan, G. Zhang, X. Wang, A facile synthesis of Br-modified g-C3N4 semiconductors for photoredox water splitting, Appl. Catal. B 192 (2016) 116–125.
[52] M.J. Frisch, G.W. Trucks, H.B. Schlegel, G.E. Scuseria, M.A. Robb, J.R. Cheeseman, G. Scalmani, V. Barone, B. Mennucci, G.A. Petersson, H. Nakatsuji, M. Caricato, X. Li, H.P. Hratchian, A.F. Izmaylov, J. Bloino, G. Zheng, J.L. Sonnenberg, M. Hada, M. Ehara, K. Toyota, R. Fukuda, J. Hasegawa, M. Ishida, T. Nakajima, Y. Honda, O. Kitao, H. Nakai, T. Vreven, J.A. Montgomery, Jr., J.E. Peralta, F. Ogliaro, M. Bearpark, J.J. Heyd, E. Brothers, K.N. Kudin, V.N. Staroverov, T. Keith, R. Kobayashi, J. Normand, K. Raghavachari, A. Rendell, J.C. Burant, S.S. Iyengar, J. Tomasi, M. Cossi, N. Rega, J.M. Millam, M. Klene, J.E. Knox, J.B. Cross, V. Bakken, C. Adamo, J. Jaramillo, R. Gomperts, R.E. Stratmann, O. Yazyev, A.J. Austin, R. Cammi, C. Pomelli, J.W. Ochterski, R.L. Martin, K. Morokuma, V.G. Zakrzewski, G. A. Voth, P. Salvador, J.J. Dannenberg, S. Dapprich, A.D. Daniels, O. Farkas, J.B. Foresman, J.V. Ortiz, J. Cioslowski, D.J. Fox, Gaussian, Inc., Wallingford CT, 2013.
[53] W. Yan, Z. Han, B. Phung, F. Faupel, K. Ostrikov, High-Voltage Insulation Organic-Inorganic Nanocomposites by Plasma Polymerization, Materials 7 (2014) 563–575.
[54] J. Cai, J. Huang, S. Wang, J. Iocozzia, Z. Sun, J. Sun, Y. Yang, Y. Lai, Z. Lin, Crafting Mussel-Inspired Metal Nanoparticle-Decorated Ultrathin Graphitic Carbon Nitride for the Degradation of Chemical Pollutants and Production of Chemical Resources, Adv. Mater. 31 (2019), 1806314.
[55] J. Chen, C.-L. Dong, D. Zhao, Y. Huang, X. Wang, L. Samad, L. Dang, M. Shearer, S. Shen, L. Guo, Molecular Design of Polymer Heterojunctions for Efficient Solar-Hydrogen Conversion, Adv. Mater. 29 (2017), 1606198.
[56] J. Liu, Y. Liu, N. Liu, Z. Han, X. Zhang, H. Huang, Y. Lifshitz, S.-T. Lee, J. Zhong, Z. Kang, Water splitting. Metal-free efficient photocatalyst for stable visible water splitting via a two-electron pathway, Science 347 (2015) 970–974.
[57] Y. Zheng, Y. Jiao, Y.H. Zhu, L.H. Li, Y. Han, Y. Chen, A.J. Du, M. Jaroniec, S. Z. Qiao, Hydrogen evolution by a metal-free electrocatalyst, Nat. Commun. 5 (2014) 3783.
[58] Y.T. Dai, Q.J. Bu, R. Sooriyagoda, P. Tavadze, O. Pavlic, T.B. Lim, Y.B. Shen, A. Mamakhel, X.P. Wang, Y.W. Li, H. Niemantsverdriet, B.B. Iversen, F. Besenbacher, T.F. Xie, J.P. Lewis, A.D. Bristow, N. Lock, R. Su, Boosting photocatalytic hydrogen production by modulating recombination modes and proton adsorption energy, J. Phys. Chem. Lett. 10 (2019) 5381–5386.
[59] K.L. Corp, C.W. Schlenker, Ultrafast spectroscopy reveals electron-transfer cascade that improves hydrogen evolution with carbon nitride photocatalysts, J. Am. Chem. Soc. 139 (2017) 7904–7912.